Published in Quarterly Journal of Engineering Geology and Hydrogeology, 2017,128-137, 2018
which should be used for any reference to this work

Long-term effects of deep-seated landslides on transportation infrastructure: a case study from the Swiss Jura Mountains

Giona Preisig

Centre for Hydrogeology and Geothermics, University of Neuchâtel, Emile-Argand 11, CH-2000 Neuchâtel, Switzerland
G.P., 0000-0001-6588-1564
Correspondence: giona.preisig@unine.ch

Abstract: Deep-seated landslides (DSLs) involve large-scale deformation and likely affect transportation infrastructure. Movement rates are in general very slow (less than a metre per year) with acceleration periods controlled by external factors such as the seasonal fluctuation of groundwater pressure. Acceleration response may change from season to season depending on hydrogeological conditions, changes in slope geometry and degradation of geological materials. More localized landslide types are associated with and develop within DSLs, such as rock falls, topples and debris slides. Management of hazards related to DSLs requires first the assessment of geological, hydrogeological and geomechanical processes. This is the starting point for developing a management strategy. This paper presents the characterization of a deep-seated landslide located in the Swiss Jura Mountains, Les Buges landslide, where a railway line, a power line and an aqueduct of regional importance cross the slide, as well as a highly frequented hiking trail beneath the landslide toe. Slide kinematics is governed by the geology and hydrogeology of the slope, which can be subdivided into two dominant bodies. A management strategy is subsequently discussed for this DSL. Les Buges is a good example illustrating that hazards related to deep-seated landslides must be tackled first of all by means of the observational method.

Deep-seated landslides (DSLs) are mass movements involving large-scale deformations that may affect the entire slope of a valley or a mountain (Fig. 1a). They comprise well-developed distinct boundaries and geomorphological features such as head scarps, tension cracks, horst-and-graben structures and listric faults in the upper slide part, and typical contractional features in the lower slide part such as thrust faults, block rotation, distortion and dilation. Lateral and at-depth boundaries are formed by shear or sliding zones governing the slide kinematics. The basal, at-depth sliding zone often presents a curvature (Agliardi *et al.* 2012; Hungr *et al.* 2014; Pánek & Klimeš 2016). DSL velocities are very slow and difficult to measure. Typical ranges include base velocities of the order of centimetres per year and peak velocities of the order of centimetres per day. Peak velocities typically occur during acceleration periods in response to external factors, such as seasonal fluctuations of groundwater pressure or nearby seismic events of significant magnitude (e.g. $M_w > 5$). For many DSLs in Switzerland, the snowmelt period coupled with intense rainfall during spring is in general able to increase groundwater pressure so that movement rates are increased at least once a year from base to peak velocities (Tacher *et al.* 2005; Bonzanigo *et al.* 2007; Preisig *et al.* 2016). These episodic accelerations are not regular because the volume of infiltrated water (i.e. recharge) may vary from year to year (Tacher *et al.* 2005; Smethurst *et al.* 2012; Elia *et al.* 2017), and mechanical and hydrodynamic properties can vary in space and time owing to movement, degradation and weakening of the sliding mass (Gischig *et al.* 2016; Preisig *et al.* 2016). The progressive failure of DSLs from first-time failures to a final collapse or not, is a very long process. In the Alps and Jura Mountains, many DSLs have been active since the end of the Pleistocene (11.5 ka) and even before. The likelihood of a DSL or a part of it evolving into a brittle, rapid large failure at the origin of a catastrophic rock collapse or debris avalanche may be estimated from the dominant characteristics. Irregular 'collapse' slides as defined by Hungr *et al.* (2014) with an irregular, steep sliding zone probably develop with time a planar, steep rupture surface, pick up speed and fail catastrophically (Fig. 1b). DSLs with a deep, curved sliding surface, 'compound slides' as defined by Hungr *et al.* (2014), will continue to show their characteristic slow, episodic movements and, under natural conditions, rarely reach extremely rapid velocities (Preisig *et al.* 2015; Eberhardt *et al.* 2016).

The management of hazards to (transportation) infrastructure and lives, associated with deep-seated landslides, is a difficult task, principally because (1) the episodic behaviour may evolve with increased slope weakening into a rapid large failure and/or (2) secondary failure mechanisms may be present, such as debris slides, rock falls and block topples. In Switzerland, numerous examples exist (Table 1). DSLs classified in Table 1 as rock compound slides or soil compound slides have shown alarming periods of activity with enhanced slope movement, increased rock falls and debris slides, preceded and/or followed by many seasons with nil levels of activity, and negligible impacts and damage. This behaviour complicates the hazard management even if it is unlikely that these types of DSLs fail catastrophically. Damage to transportation infrastructure (regional roads) and buildings caused by the episodic movement of the Campo Vallemaggia (TI), La Frasse (VD) and Montagnon (VS) deep-seated landslides reached unacceptable levels requiring a mitigation strategy by means of deep drainage, through tunnels or pumping wells with the aim of increasing the DSLs' shear strength by reducing groundwater pressures. A mitigation strategy for the Braunwald (GL) and the Brienz (GR) landslides is currently under consideration. DSLs classified in Table 1 as irregular 'collapse' slides have failed or will fail in the near future. The management of both the Preonzo (TI) and the Randa (VS) rockslides required the implementation of early warning systems accompanied by an evacuation plan for protecting lives, as well as the construction of embankments for protecting buildings and transportation infrastructure. The lower part of the Moosfluh slide (VS) will fail in the upcoming years. Its movement is monitored by satellite (interferometric synthetic aperture radar;

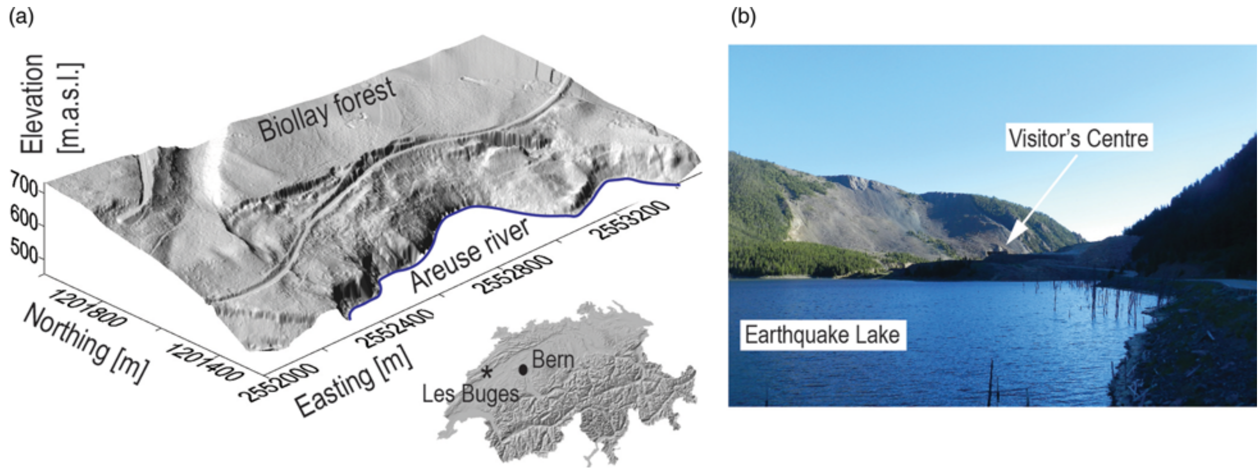

Fig. 1. (**a**) Three-dimensional view of the digital elevation model *swissALTI3D* (swisstopo 2017) for Les Buges deep-seated landslide (DSL) with its location. Typical geomorphological features of DSLs are well recognized: headscarp, half-grabens and lateral boundaries, as well as the location of anthropogenic features, such as the railway track. (**b**) The Madison Canyon DSL (Montana, USA) evolved into a catastrophic collapse slide in response to a magnitude 7.5 earthquake. The visitors centre is built on collapse deposits and is *c.* 25 m wide. (Refer to Wolter *et al.* (2016) for more details on the Madison Canyon landslide.)

InSAR) and field (global positioning system; GPS) instrumentation. The management of this slide required the closure of touristic hiking trails and a sophisticated early warning system for anticipating the closure of a gondola located in the upper part of the unstable slope. It should be noted that the foundations of the gondola station are designed to support decametre-scale displacements. A common point for all the afore-mentioned DSLs (references are listed in Table 1) is that the use of the observational method (i.e. characterization and monitoring) permitted the development of a coherent strategy of hazard management. This is the principal scope of the present study, which aims to describe the main geological, hydrogeological and geomechanical characteristics of Les Buges deep-seated landslide and illustrate how a detailed understanding is indispensable for managing hazards.

Study area: Les Buges deep-seated landslide

Les Buges deep-seated landslide (DSL) is located in the Swiss Jura Mountains (Fig. 1a), in the territory of the town of Boudry, Canton of Neuchâtel. It develops on the left slope of the Areuse gorges between elevation 450 and 650 m above sea level (a.s.l.) in a forest environment (beechwood). The Areuse gorges cut across the first anticline of the Jura Mountains and their genesis is related to glacial overdeepening owing to repeated advances and retreats of the

Table 1. *Characteristics of different types of deep-seated landslides in Switzerland and their management strategy*

Name and location	Classification according to Hungr *et al.* (2014)	Volume (million m^3); base/peak velocity ($m\ a^{-1}$); dip, sliding zone (°); catastrophic rupture (season, year)	Hazards; risk management	Example references
Campo Vallemaggia (TI)	Rock compound slide	800 mio m^3; <0.02/>0.1 $m\ a^{-1}$; <25°; unlikely	Infrastructure damage or valley-blocking; mitigation (drainage adit, 1995)	Bonzanigo *et al.* (2007), Eberhardt *et al.* (2007)
La Frasse (VD)	Clay–silt compound slide	73 mio m^3; <0.05/>0.7 $m\ a^{-1}$; <15°; unlikely	Infrastructure damage or valley-blocking; mitigation (drainage adit 2009)	Tacher *et al.* (2005)
Montagnon (VS)	Rock compound slide	150 mio m^3; unknown/>0.1 $m\ a^{-1}$; <15°; unlikely	Infrastructure damage; mitigation (deep pumping wells and drainage adit)	Parriaux *et al.* (2010)
Braunwald (GL)	Clay–silt compound slide	50–60 mio m^3; <0.01/>0.05 $m\ a^{-1}$; <10°; unlikely	Infrastructure damage or debris slides from toe; mitigation in consideration	Frank & Zimmermann (2000)
Brienz (GR)	Clay–silt compound slide	Unknown; <0.1/>0.5 $m\ a^{-1}$; <20°; unlikely	Infrastructure damage or valley-blocking; mitigation in consideration	Canton Grisons (2015)
Randa (VS)	Rock irregular 'collapse' slide	30 mio m^3; <0.01/>0.03 $m\ a^{-1}$; >30°; spring 1991	Infrastructure damage, fatalities; early warning systems and protective structures	Sartori *et al.* (2003), Gischig (2011)
Preonzo (TI)	Rock irregular 'collapse' slide	0.21 mio m^3; <0.1 $m\ a^{-1}$/>1 cm day^{-1}; >40°; spring 2012	Infrastructure damage, fatalities; early warning systems and protective structures	Loew *et al.* (2017)
Moosfluh (VS)	Rock irregular 'collapse' slide and/or rock block topple	150 mio m^3; <0.1 $m\ a^{-1}$/>30 cm day^{-1}; >30°; in progress	Infrastructure damage, fatalities; early warning systems and closure of areas	Strozzi *et al.* (2010), Grämiger *et al.* (2017)

Classification and dip of the basal sliding zone are good indicators of whether the DSL might undergo catastrophic failure or not. It should be noted that average values of dips are considered, as well as examples of peak velocities for 'collapse' slides representative for (1) seasonal acceleration events long before collapse (Randa), (2) abnormal acceleration 2 years before collapse (Preonzo) and (3) acceleration towards collapse (Moosfluh).

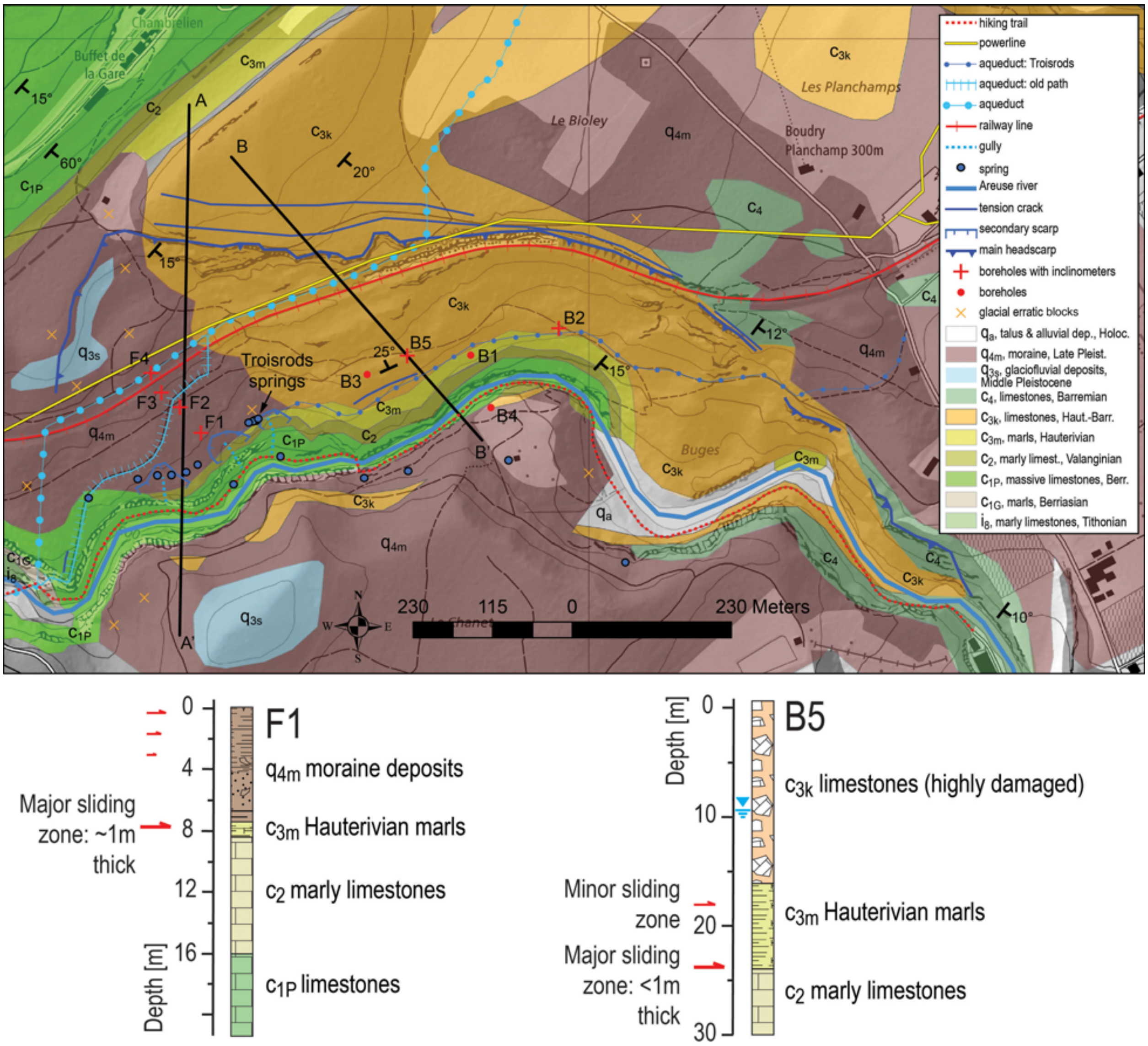

Fig. 2. Geological map with structural, geomorphological and hydrogeological features, as well as location of (transportation) infrastructure for Les Buges deep-seated landslide with representative boreholes for (F1) the west and (B5) east slide bodies. Data from Meia & Becker (1976), GeoConsult (1985, 1994) and Meia (1996) were compiled, processed and completed with new field acquisitions to produce this figure.

Rhone glacier during the Pleistocene and erosion by the Areuse River during the Holocene (Pasquier *et al.* 2013). The railway line connecting the city of Neuchâtel to the Travers Valley and to Pontarlier (France) passes through this slide, as do the aqueduct supplying water to the city of Neuchâtel and a power line (Fig. 2). A touristic hiking trail is located at the slope's foot. In the absence of a detailed assessment, natural hazards related to this DSL might include the following: (1) movement acceleration to (partial) slope collapse blocking the gorges and forming a dammed lake; (2) damage to (transport) infrastructure owing to slow slope deformation, rock falls and topples in the upper part of the slide; (3) debris slides from the DSL's toe to the river level; (4) rock falls or topples in the gorges.

Les Buges deep-seated landslide has been known for a long time. The name 'Les Buges' probably originates from the French term 'bouger', which means 'to move'. The unstable character of this slope was first mapped in the seminal work of Schardt & Dubois (1902) on the geology of the Areuse gorges. From 1977 to 1996, cantonal geologist J. Meia launched and supervised a series of detailed investigations (Meia 1996) because of enhanced slope activity, especially in the lower part, where a series of debris slides occurred. The detailed investigations included drilling of boreholes (Meia 1996), inclinometers (GeoConsult 1994) and geophysical surveys (GeoConsult 1985). This crisis was probably initiated by significant water leakages from the aqueduct supplying water to the city of Neuchâtel in 1977, associated with major snowmelt and rainfall periods during the winter. Leakages were observed in 15 cracks, whose opening was probably induced by the natural episodic movement of the deep-seated landslide. The aqueduct path was adapted because of this crisis (Fig. 2). In November 2008, the growth of a tension crack located below the railway line caused the formation of a small cavity in the ground with loss of ballast. Recently, a technical report has been produced (CSD Ingénieurs 2016) to (1) categorize the various natural hazards accompanying the DSL's slow deformation, (2) present an inventory of infrastructure at risk and (3) perform hazard and risk analyses by means of risk matrices.

The present study follows the 2016 technical report and, as indicated above, focuses on a scientific description of geological, geomechanical and hydrogeological processes governing the instability of deep-seated landslides, and their long-term impacts on (transportation) infrastructure. For this, boreholes and measurements made by Meia (1996) and GeoConsult (1985, 1994) at Les Buges have been compiled, processed, interpreted and completed by new field acquisitions in 2016 and 2017. In addition to

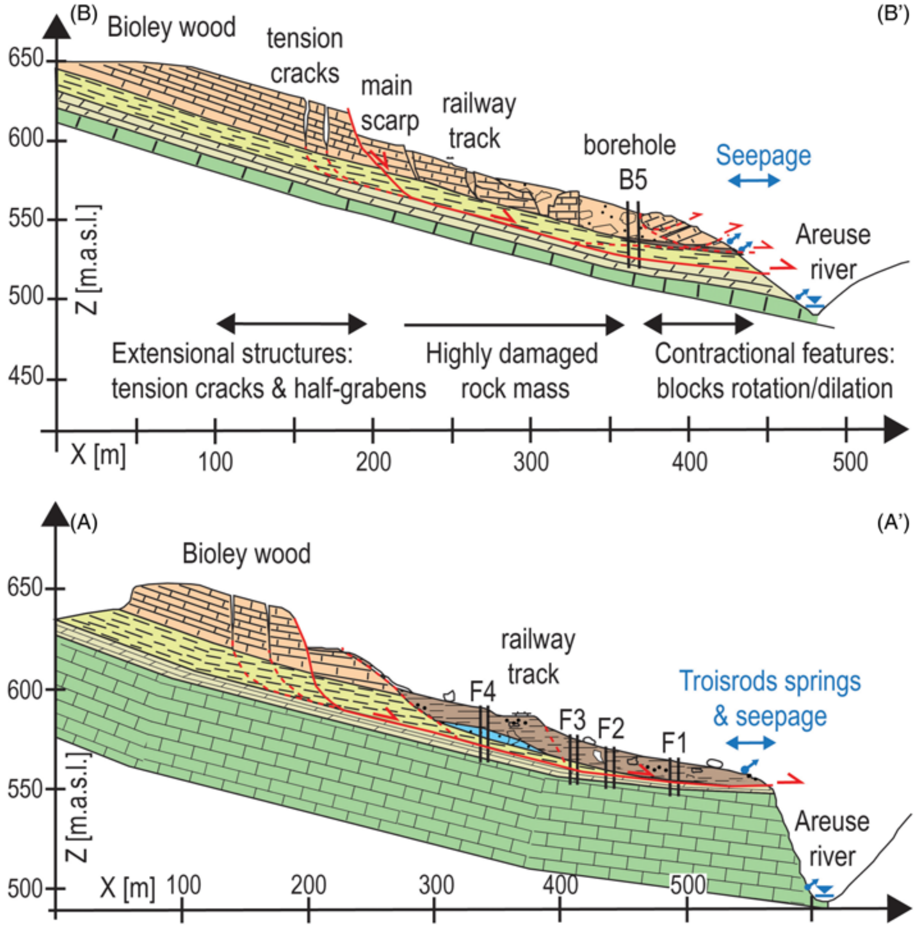

Fig. 3. Geological cross-sections representative for the (A–A') west and (B–B') east slide bodies. Location is indicated in Figure 2.

geological field observations, these include a series of electrical resistivity tomographies for geological characterization and the calculation of the DSL's thickness and volume; as well as the installation of equipment for monitoring groundwater pressure in the basal sliding zone and flow rates from springs located in the lower part of the slide. These data permit calculation of the water balance of the landslide.

Slide geology

The stratigraphic sequence is a succession of medium strong to very strong limestones interbedded with weak marl layers, gently dipping to the SE. In the west part of the slope, Quaternary deposits overlie this sequence. They include at the base discontinuous glaciofluvial gravels superimposed by moraine deposits, which are highly heterogeneous, comprising plastic clay layers interbedded with silty or clayed gravels. Figure 2 is a geological map showing the principal geomorphological features of the slide and (transport) infrastructure. The lateral extent of Les Buges DSL is delineated by the main headscarps and tensile cracks (upper and lateral boundaries) and the Areuse gorges (lower boundary). From surface geology, it can be easily recognized that the DSL comprises at least two dominant bodies: in the east body, the slide affects the c_{3k} Hauterivian–Barremian limestones, commonly known as the Pierre Jaune de Neuchâtel, whereas the west body is principally composed of q_{4m} moraine deposits. Eight boreholes were drilled into the deep-seated landslide, six of which have been equipped for inclinometer measurements (Fig. 2). Figure 2 also schematizes the geological interpretation of two boreholes, B5 and F1, representative for the east and west slide bodies, respectively. Inclinometer data for borehole B5 indicate that the major at-depth sliding zone is situated at the base of Hauterivian marls (c_{3m}). Here, the deep-seated landslide thickness is about 24 m, including 8 m of c_{3m} marls overlain by 16 m of highly damaged c_{3k} limestones. In borehole F1 the base of the sliding zone has also been identified at the bottom of Hauterivian marls (c_{3m}), matching here a depth of about 8.5 m. The marls are herein very thin (i.e. less than 1 m), overlain by about 7.5 m of q_{4m} moraine deposits with at their base a plastic clay layer of at least 0.5 m thickness (see cross-sections in Fig. 3). This horizon completes the major sliding zone for this part of the DSL. Geophysical data obtained by means of seismic (GeoConsult 1985) and geoelectric surveys (this study) complement the boreholes data, and allowed us to generate by interpolation a map of total DSL thickness and to calculate the DSL volume, which is about 9 million m^3 (mio m^3) (Fig. 4a). In designing Figure 4a, the landslide base has been interpreted at the bottom of Hauterivian marls at most of the measurement points, with the exception of the west end, where the landslide base has been interpreted at the bottom of Quaternary deposits.

Five dominant subvertical fracture sets are identifiable in the field (Rey 2015). The main headscarp and tension cracks (Figs 3 and 4b) arise from the reactivation of fracture sets oriented WNW–ESE and WSW–ENE. Half-graben structures and a highly damaged rock mass characterize the east slide body, which is in the lower part affected by rotational movement of rock blocks (Fig. 3). This is observable in the field because the dip of bedding planes is reversed compared with the regional dip (Fig. 2). The dip of the basal sliding zone matches the dip of c_{3m} Hauterivian marls and is about 15° to the SE. According to the updated Varnes classification of landslide types (Hungr *et al.* 2014), the east body of Les Buges DSL is classified as a rock compound slide.

Figure 3 (lower part) shows a schematic cross-section of the west slide body. It should be noted that the c_{3m} Hauterivian marls become thinner towards the west and they are probably absent in the proximity of the Troisrods springs. Discontinuous lenses of q_{3s} glaciofluvial gravels may be found at the base of the Quaternary sequence, especially in the upper part. These deposits correspond to

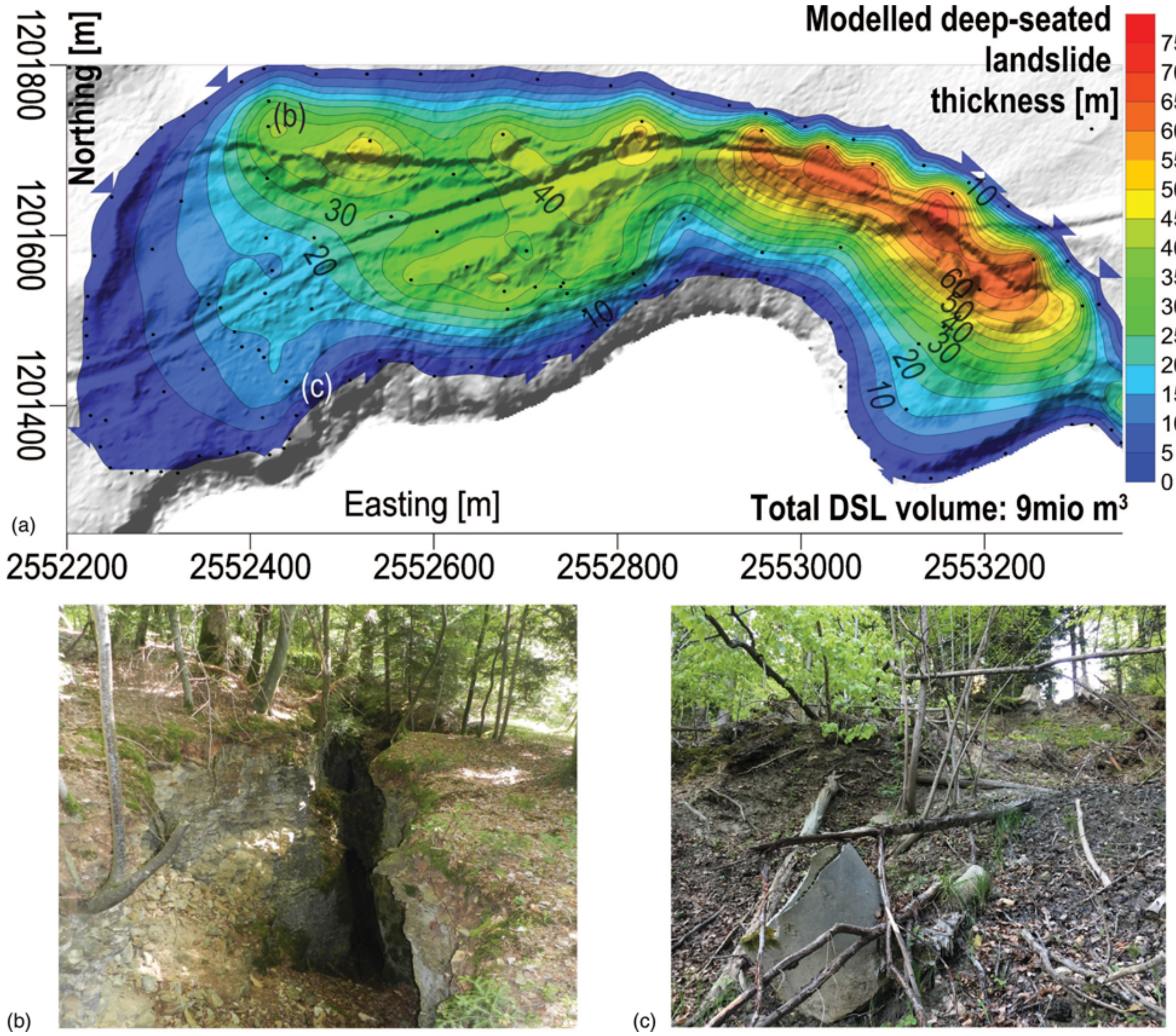

Fig. 4. (**a**) Modelled thickness and volume of Les Buges deep-seated landslide (DSL). Black points indicate locations of observational data (boreholes, geophysical surveys and field observations) used to constrain the interpolation. Data from Meia & Becker (1976), GeoConsult (1985, 1994) and Meia (1996) were compiled, processed and completed with new field acquisitions to produce this map. (**b**) Tension crack in the upper part of the DSL (the crack is *c.* 2 m wide). (**c**) Sliding mass (moraine deposits) at the toe of the west slide body. The accumulation and erosion of debris owing to the DSL movement should be noted (the photograph is *c.* 10 m deep). Location of photographs is indicated in (**a**).

GW/GP soils according to the unified soil classification system (USCS) with high values of hydraulic conductivity: 10^{-3}–10^{-2} m s^{-1} (SIA VSS 2011). Moraine deposits are highly heterogeneous, comprising silty or clayed gravels interbedded with clay horizons. Many gravels have an Alpine origin (i.e. they are composed of gneiss of the Aar massif) and have been transported from the Alps by the Rhone glacier. Indeed, many glacial erratic blocks are found on the moraine deposits (Fig. 2). A major silty clay layer is found at the base of moraine deposits just above the c_{3m} Hauterivian marls (Fig. 3c). According to the USCS, this corresponds to a CL/CH or CM soil with low frictional angle of 10–20° (SIA VSS 2011). This clay horizon together with the marls layer forms the major zone of weakness in the west slide body, which is considered as a rock–clay compound slide.

Slide kinematics and geomechanical behaviour

As proposed by Leroueil *et al.* (1996), the kinematics history of an unstable slope can be subdivided into four stages: pre-failure, first-time failure, post-failure and reactivation. Pre-failure history at Les Buges is related to repeated advances and retreats of the Rhone glacier in the Areuse gorges during the Pleistocene with valley overdeepening, glacial loading–unloading cycles accompanied by rock mass fatigue, weathering of pre-existing planes of weakness and propagation of new fractures. By studying paraglacial rock slope instabilities in the Aletsch area (Valais, Switzerland), Grämiger *et al.* (2017) indicated that glacial loading and unloading enhances the criticality of fractures rather than promoting damage. In the course of the pre-failure stage at Les Buges, slope pre-conditioning in the form of propagation of new fractures or plastic responses was thus probably related to hydrogeological, thermal and other destabilizing processes during interglacial periods. Slope de-buttressing was accelerated by glacial and fluvial erosion of c_{3m} Hauterivian marls in the gorges, probably triggering first-time failures of Les Buges DSL. This followed the last deglaciation event in the Areuse gorges (late Pleistocene–early Holocene) at about 11.5 ka. Close to the east boundary of the DSL, a rock block of about 90 000 m^3 is detached from the main headscarp by 30 m. Sliding here looks translational, and if constant velocity owing to creep is assumed, this results in an average velocity of 3 mm a^{-1} for this part of the slope. Residual strength and properties are in general considered from the post-failure stage onward.

The observational window obtained by repeated inclinometer measurements (Geoconsult 1994) corresponds to reactivation stages. Figures 5 and 6 present inclinometer data for boreholes F1 and B2, which are characteristic for the west and east slide bodies, respectively. Geological formations as interpreted from borehole logs are illustrated on the left. In both cases, the major basal sliding zone develops at the bottom of Hauterivian marls. Other minor sliding zones appear in the sliding mass. For borehole F1, inclinometer data indicate that the basal sliding zone is about 1 m thick and thus comprises the silty clay horizon at the bottom of moraine deposits. For borehole B2, inclinometer data also indicate the rotational movement of limestone blocks (sliding mass). Figures 5 and 6 also present observed displacements (at different depth levels) and calculated velocities as a function of time with precipitation and snow cover recorded in the Areuse gorges (Meteoswiss 2017). Measured displacements indicate different kinematics for the west and east slide bodies. Borehole B2 has been affected by a deformation of about 2 cm in 10 years, corresponding to an average velocity of about 2 mm a^{-1}. This is in line with the afore-mentioned velocity for this part of the DSL. Velocities presented in Figure 6 also suggest a constant movement. Some fluctuations are visible, but are probably related to measurement or processing errors. These extremely low velocities probably result from creep at the base of the Hauterivian marls, governing the kinematics of the east slide body. In contrast, the west slide body (Fig. 5) shows episodic movement characterized by two acceleration events with peak velocities of about 2.5 and 4 cm a^{-1} identifiable between 1980 and 1983. For this period, base velocities are in the range of or lower than 1 cm a^{-1}. It should be noted that after the second acceleration event in 1982, the inclinometer tube was sheared at a depth of 8 m, stopping its functionality. Figure 5 also suggests that acceleration events in the west slide body occur during the winter–spring period when groundwater recharge is favoured by rainfall, snowmelt and nil activity of vegetation. Groundwater pressure is thus increased in the Hauterivian marls and moraine deposits, diminishing both the effective stress and the shear strength in sliding zones, and favouring shear slip. Peak velocities observed for the west slide body are slow to very slow according to the landslide velocity scale (Hungr *et al.* 2014), and are in the lower range compared with peak velocities of other deep-seated landslides in the Swiss Alps (Table 1). However, these velocities remain one order of magnitude greater than velocities measured in the east body.

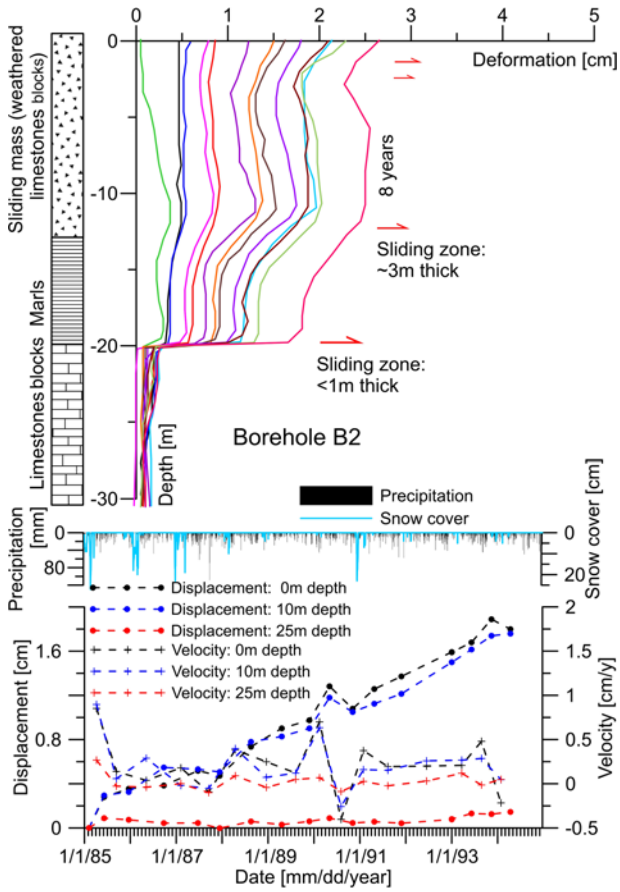

Fig. 6. Deformation as a function of (above) depth and (below) time derived from repeated inclinometer measurements (Geoconsult 1994) for borehole B2 spanning a period of about 8 years. In the upper plot, interpreted geology is shown along the depth axis; the lower plot integrates recorded precipitation and snow cover (Meteoswiss 2017) and calculated velocities.

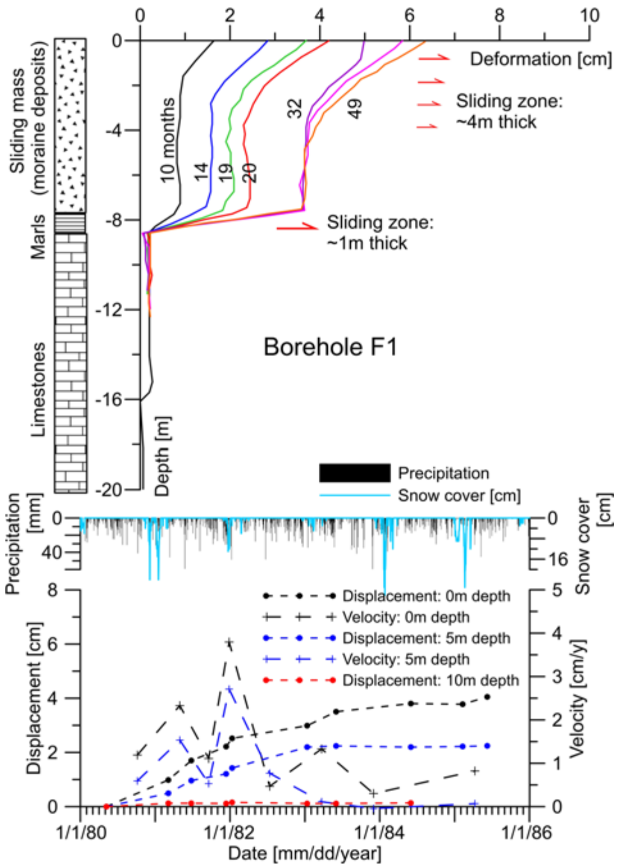

Fig. 5. Deformation as a function of (above) depth and (below) time derived from repeated inclinometer measurements (Geoconsult 1994) for borehole F1. In the upper plot, interpreted geology is shown along the depth axis and numbers on curves are months after inclinometer installation (5 May 1980). The lower plot integrates recorded precipitation and snow cover (Meteoswiss 2017) and calculated velocities. It should be noted that the inclinometer tube broke more or less before the third peak.

Slide hydrogeology

Figure 2 illustrates the location of springs in proximity to or within the deep-seated landslide. Springs and seepage zones originate from different aquifer layers: (1) at the river level, karstic springs relate to c_{1P} Berriasian limestones; (2) a seepage zone spreads the DSL more or less from east to west where c_{3m} Hauterivian marls crop out; (3) many springs are located in the west slide body at the downslope end of moraine deposits. Here, springs are collected in a reservoir (Troisrods springs) and served in the past to supply water to a part of Boudry. Groundwater infiltration is facilitated in the upper part of the slope by the presence of permeable glaciofluvial gravels and open tension cracks (Fig. 2).

The criticality of many DSLs is related to groundwater overpressures owing to the interaction between different aquifer

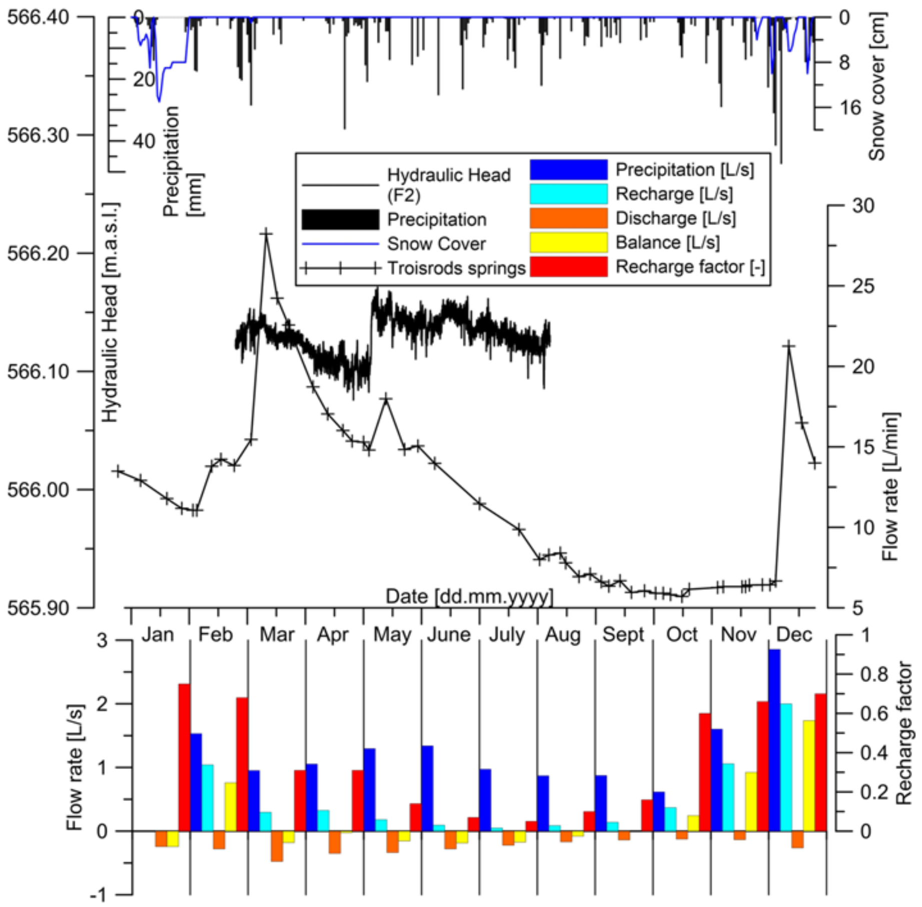

Fig. 7. Above; precipitation, snow cover, hydraulic head in the sliding zone (borehole F2) and flow rate at Troisrods springs; below; monthly water balance for the west slide body as a function of time for the year 2017.

layers. Bonzanigo *et al.* (2007) suggested that at the Campo Vallemaggia DSL increasing groundwater pressure in a deep aquifer located below the basal sliding zone was responsible for a pulsing behaviour; that is, opening of fractures and subsequent quick drainage resulting in reduced slope strength and movement acceleration. Tacher *et al.* (2005) indicated that at La Frasse DSL, two-thirds of the inflow comes from aquifer layers bordering the slide. Deep-seated landslides involve a groundwater catchment area that is often much larger than the slide extent. Moreover, groundwater recharge from precipitation highly depends on the precipitation type and vegetation activity. Response to precipitation is thus, to some degree, unique for each DSL, and this explains why the relationship between precipitation and movement is often not clear or there is no correlation. Monitoring springs and seepage flow rates is a practical way to understand DSL response to precipitation by means of a water balance. For the west body of Les Buges DSL, the mean (exfiltrating) volumetric flow rate is about 0.3 l s^{-1} for the period November 2016 to September 2017 (0.24 l s^{-1} measured at the Troisrods spring and 0.06 l s^{-1} estimated from the seepage area). A volumetric flow rate of about 0.9 l s^{-1} is obtained if recorded precipitation at a meteorological station located about 1 km from the slide (Meteoswiss 2017) is integrated over a surface matching more or less the extent of glaciofluvial gravels and tension cracks in the upper part of the west slide body. The water balance for this part of the slide is thus closed if a recharge factor of one-third is applied to precipitation (i.e. an infiltrating flow rate of 0.3 l s^{-1}). This recharge factor comprises evapotranspiration and water runoff and is in agreement with values commonly observed for the Jura Mountains (Menzel *et al.* 1999). This also indicates that at Les Buges there are no deep groundwater contributions.

The upper panel of Figure 7 illustrates (1) precipitation and (2) snow cover recorded at the nearby meteorological station (Meteoswiss 2017), (3) (piezometric) hydraulic head in the sliding zone (borehole F2) and (4) flow rates of Troisrods springs as a function of time. The lower panel of Figure 7 shows monthly water balance computed for the west slide body by applying a time-varying recharge factor typical for the Swiss Jura Mountains (Menzel *et al.* 1999). Evapotranspiration controls the variation of the recharge factor, which tends to unity for the period December–February. From Figure 7, it can be seen how the seasonal activity of vegetation, rather than precipitation, regulates the volume of infiltrated water (effective recharge) and thus groundwater pressure in the west slide body. Peak yearly flow rate at Troisrods springs follows the snowmelt period. Any significant rainfall and/or snowmelt event in the period November–April is thus efficient in recharging the groundwater system and increasing pore pressures in the basal sliding zone of the west slide body, whereas from May to early October vegetation activity limits water infiltration and reduces groundwater flow and seepage to base levels. This process is at the origin of the episodic movement of the west part of Les Buges deep-seated landslide as presented in Figure 5.

Long-term effects on (transportation) infrastructure and conclusions

According to the updated Varnes classification of landslide types (Hungr *et al.* 2014), the east body of Les Buges DSL is classified as a rock compound slide, whereas the west body is considered as a rock–clay compound slide. These types of slides present a basal rupture zone that develops within or at the bottom of a weak layer in the lithostratigraphy, as well as a steep main scarp and horst-and-graben structures in the upper part of the slide. Furthermore, slide motion is kinematically possible if and only if it is accompanied by internal distortion of the sliding mass (Hungr *et al.* 2014). Downhill movement is slow to very slow and results from a combination of intrinsic material creep under gravitational loading and episodic reduction of resisting forces (shear strength), in general owing to groundwater pressure variations. These types of slides are unlikely

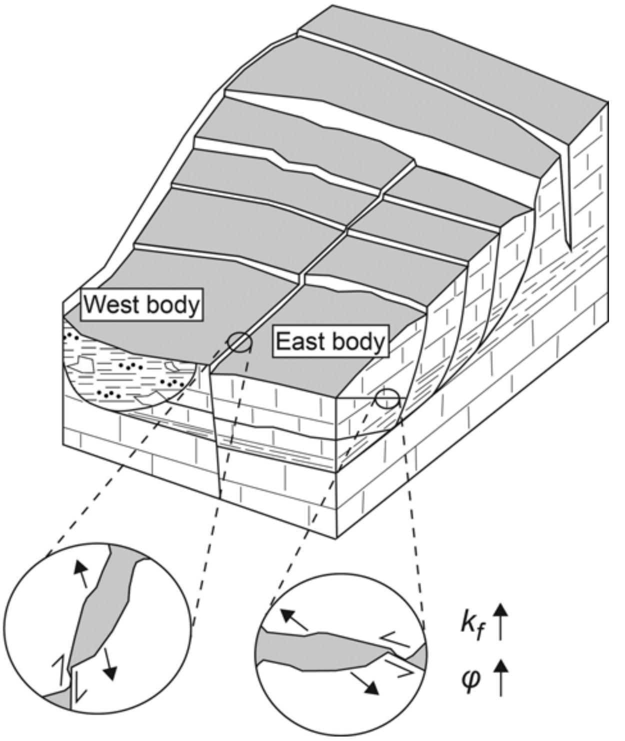

Fig. 8. Three-dimensional illustration of west and east slide bodies with drawings showing effects of shear dilation on fracture and rock permeability, as well as on friction angle.

to speed up to a rapid, catastrophic failure. Indeed, if any sliding episode might imply a reduction of resisting forces (e.g. peak to residual rock or soil properties), movement is counteracted by a change in slide geometry. As the basal sliding zone is non-planar (concave) and often rough, this implies a reduction of gravity-based driving forces and dilation in the lower part of the slide. Dilation is often accompanied by an increase in friction and permeability (Fig. 8). The first slows down or inhibits movement; the second promotes drainage, decreasing the likelihood of shear strength reduction owing to increasing groundwater pressures. Les Buges DSL is a good example of this, and the lower part of the east slide body is used to illustrate the effect of shear dilation on rock mass permeability and landslide stability. The relationship between shear displacement (U_s) and dilation angle (ψ) given by Barton *et al.* (1985) is practical for quantifying the increase of the mechanical aperture of a fracture (Δa_m) with shear dilation:

$$\Delta a_m = U_s \tan \psi. \tag{1}$$

The increase of mechanical aperture (i.e. considering fracture roughness) is then converted into an increase of hydraulic aperture (Δa_h) (i.e. assuming smooth surfaces) via the empirical abacus provided by Barton *et al.* (1985) defining the ratio of a_m/a_h. This ratio typically tends to unity for fractures with low roughness and high hydraulic aperture (>0.1 mm) and to five for fractures with pronounced roughness and low hydraulic aperture. The resultant hydraulic aperture of a fracture after shear dilation is thus $a = a_{init} + \Delta a_h$, where a_{init} is the initial hydraulic aperture. Equivalent permeability tensors are practical for describing the permeability of fractured rock masses. They are obtained by considering in three dimensions the geometrical and conductive (cubic law) properties of each fracture family characterizing the rock mass:

$$\mathbf{k} = \sum_{i=1}^{m} \frac{f_i a_i^3}{12} (\mathbf{I} - \mathbf{n}_i \otimes \mathbf{n}_i) = \begin{bmatrix} k_{xx} & k_{xy} & k_{xz} \\ k_{yx} & k_{yy} & k_{yz} \\ k_{zx} & k_{zy} & k_{zz} \end{bmatrix} \tag{2}$$

where for each fracture family i, a is the fracture hydraulic aperture, f is the frequency of the fracture family i, $\mathbf{I}$ is the identity matrix, $\mathbf{n}$ is the unit vector normal to the fracture family i, and $\otimes$ denotes a tensor product. m is the total number of fracture families. The rightmost part of equation (2) expresses the tensor in its matrix form. It should be noted that the eigenvalues of a permeability tensor match the magnitude and direction of maximum (k_{max}) and minimum (k_{min}) permeability (Király 1969). Gains in rock mass permeability in response to fracture dilation are illustrated by the ratio between components of the equivalent rock mass permeability tensor prior to dilation ($\mathbf{k_{init}}$) and with dilated apertures ($\mathbf{k}$).

Table 2 presents gains in rock mass permeability for the c_{3k} Hauterivian–Barremian limestones (Pierre Jaune de Neuchâtel) in the lower part of the east slide body if a shear displacement of about 3 mm a^{-1} is applied to the dominant fracture families. It should be noted that the analysis uses a conservative dilation angle $\psi = 1°$ and a conservative ratio of $a_m/a_h = 5$. In the short term (<10 years), dilation effects may be neglected, but in the long term (>100 years) shear dilation of fractures may increase rock mass permeability by about three orders of magnitude. Such a gain is in agreement with values commonly found during hydraulic stimulation treatments (Preisig *et al.* 2014). The impact of dilation on the stability of the east slide body is finally exemplified by considering the factor of safety (FoS) and the Mohr–Coulomb failure criterion:

$$\text{FoS} = \frac{\text{RF}}{\text{PF}} = \frac{c + (\sigma - p) \tan \varphi}{\tau} \tag{3}$$

where RF are stresses resisting movement (shear strength), PF are stresses promoting movement, c is cohesion, σ is total stress, p is water pressure, φ is the frictional angle and τ is shear stress. In the long term, the enhancement of rock mass permeability in response to dilation leads to well-drained groundwater flow conditions inhibiting the appearance of large water pressures during the winter period. This stops the reduction of both the effective stress and shear strength. Resisting forces thus remain constant during the winter period, ensuring slope stability. Moreover, shear dilation increases the frictional angle by $\varphi = \varphi_{init} + \psi$, where φ_{init} is the frictional angle

Table 2. *Gains in rock mass permeability in response to shear dilation for limestones in the lower part of the east body by supposing a shear displacement of about 3 mm a^{-1} applied to the principal fracture families and using conservative dilation angle ($\psi = 1°$) and ratio of mechanical to hydraulic aperture ($a_m/a_h = 5$)*

Fracture family	Initial hydraulic aperture (mm)	Shear displacement on fracture (mm a^{-1})	Stimulation of mechanical aperture (mm a^{-1})	Hydraulic aperture 1 year (mm)	Hydraulic aperture 10 years (mm)	Hydraulic aperture 100 years (mm)
1	0.06	2.6	0.045	0.069	0.151	0.967
2	0.06	2.6	0.045	0.069	0.151	0.967
3	0.05	1.5	0.026	0.055	0.102	0.574
4	0.025	1.5	0.026	0.03	0.077	0.549
5	0.02	4×10^{-6}	7×10^{-8}	0.02	0.02	0.02

$$\text{Ratio at 1 year} = \begin{bmatrix} (k/k_{\text{init}})_{xx} & (k/k_{\text{init}})_{xy} & (k/k_{\text{init}})_{xz} \\ (k/k_{\text{init}})_{yx} & (k/k_{\text{init}})_{yy} & (k/k_{\text{init}})_{yz} \\ (k/k_{\text{init}})_{zx} & (k/k_{\text{init}})_{zy} & (k/k_{\text{init}})_{zz} \end{bmatrix} = \begin{bmatrix} 1.4 & 1.5 & 0 \\ 1.5 & 1.5 & 0 \\ 0 & 0 & 1.5 \end{bmatrix}, \text{ ratio at 10 years} = \begin{bmatrix} 12 & 14 & 0 \\ 14 & 16 & 0 \\ 0 & 0 & 14 \end{bmatrix}, \text{ ratio at 100 years} = \begin{bmatrix} 2878 & 3669 & 0 \\ 3669 & 4046 & 0 \\ 0 & 0 & 3656 \end{bmatrix}.$$

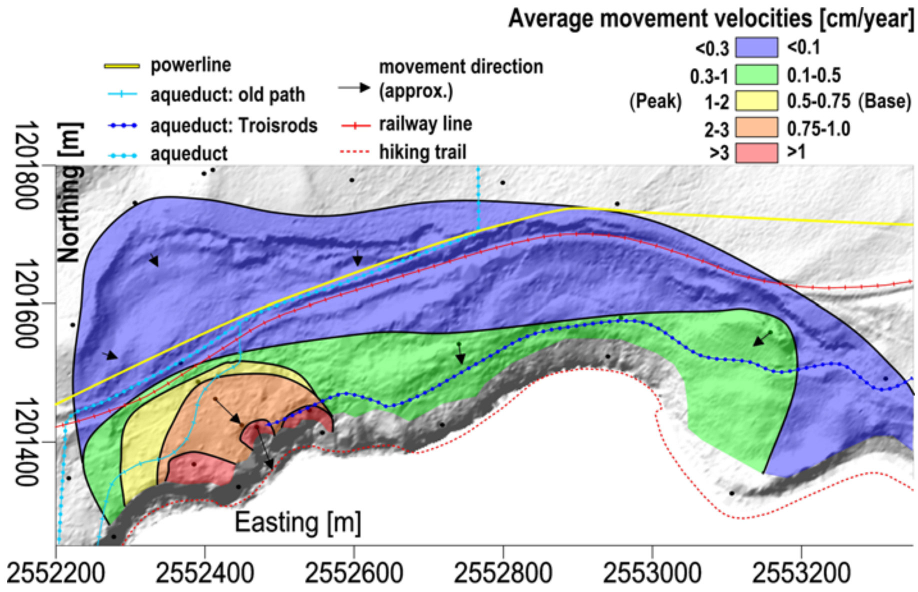

Fig. 9. Schematic map synthetizing peak and base average movement velocities for Les Buges deep-seated landslide with location of (transportation) infrastructure. Black points indicate locations of observational data.

prior to a dilation event. This process further increases shear strength and slope stability. The analysis presented above confirms field observations that the kinematics of the east slide body is governed by creep along the basal sliding zone regardless of groundwater pressure fluctuations. This is not valid for the west slide body, principally because dilation effects on permeability are negligible in soils compared with rocks. Herein, the typical slow (episodic) movement will probably continue without developing velocities greater than several centimetres per day. Processes such as catastrophic failure with formation of a dammed lake in the Areuse gorges are thus unlikely. However, this does not mean that hazards can be underestimated. Figure 9 is a map of average movement velocities derived from inclinometer data and field observations, showing also the location of (transportation) infrastructure. Average movement velocities are colour-coded according to base and peak velocities. The different behaviour between the west and east slide bodies is also observable in Figure 9, with the west body showing greater magnitude and amplitude of velocities owing to shear strength reduction as a result of groundwater pressure variations. Peak velocities in the range of centimetres per year are usually encountered between November and April in the lower part of the west body, whereas during the rest of the year vegetation activity limits water infiltration bringing the west body to base velocities. As discussed above, the east body shows more or less constant creep velocities in the range of millimetres per year. From Figure 9, it can be seen that the principal (transportation) infrastructure at risk of damage (i.e. the railway line, power line and aqueduct) is located in the upper part of the slide and is subject to a hazard of very low intensity (slow movement of a few millimetres per year). These velocities do not represent a major hazard for this infrastructure and the optimum management strategy is a periodical maintenance in the case of damage, such as occasional losses of track ballast owing to crack enlargements, in particular in the east body where the railway line encounters the main scarp and tension cracks. It is interesting to note that infrastructure located in areas where Les Buges DSL reaches peak velocities greater than 2 cm a^{-1} (i.e. the old aqueduct path and Troisrods aqueduct) has been damaged by the slide movement and subsequently abandoned. The path of the regional aqueduct has been relocated after a major crisis in 1977 (Fig. 9). Movement velocities greater than a few centimetres per year are thus a good indicator that the landslide management must go beyond simple maintenance. In such a case, monitoring measures and the planning of a mitigation strategy may be necessary to prevent major damage or even loss of the affected infrastructure. Slow downhill movement is also responsible for the degradation of the sliding mass with the emergence of more localized hazards such as rock block topples, local collapses and debris slides. At Les Buges, toppling of rock blocks is possible in the upper slide part, in particular where the railway line is just below the main scarp. Other toppling events or local collapses are possible for horst blocks, especially in the east part of the slide (see, for instance, the horst block with a movement arrow at the right of Fig. 9), or in the Areuse gorges. At these points, tension cracks have been equipped by the author to perform repeated extensometry measurements to monitor behaviour of cracks and rock blocks. Erosion and accumulation of debris in depressions and/or floors of gullies occurs at the toe of the west slide body (red areas in Fig. 9), as shown in Figure 4c. Debris accumulation may evolve during an exceptional precipitation event into a debris slide jeopardizing the hiking trail in the Areuse gorges. For security, at a major gully, the hiking trail has been replaced by a footbridge in 2010. The DSL toe has also been equipped for extensometry measurements to monitor the movement of debris accumulations.

Les Buges is also a good example showing that reliable forecasts and correct management of deep-seated landslides can be achieved only by the observational method (Hungr *et al.* 2014; Smethurst *et al.* 2017). With a small number of indicators (see, for instance, Table 1), a deep-seated landslide can be correctly classified, which is critical information for forecasting whether a slow-moving DSL may pick up speed and fail catastrophically (e.g. collapse versus compound slides). Les Buges is also a good example showing that the relationship between precipitation and movement is oversimplified for understanding the coupling between hydrogeology and geomechanics in landslides. In a forest environment, vegetation activity regulates water infiltration into aquifer layers. The amount of infiltrated water is strongly decreased between late spring and early autumn at Les Buges, whereas during the rest of the year, and especially in winter, water infiltration is at the origin of the episodic movement of the west slide body. Destabilization is particularly effective if significant snowmelt occurs when vegetation is still at nil levels of activity. Another critical interaction restraining the relationship between precipitation and movement is the coupling between shear dilation and permeability. On one hand, shear slip is accompanied by dilation with increasing permeability and friction angle. Both increases favour the stability of the slope, as they promote groundwater drainage and inhibit movement. As shown above, the gain in permeability owing to dilation may be significant in changing the hydrogeological conditions of a part of the slope from undrained to well drained. On the other hand, other kinematical behaviours such as toppling can decrease permeability leading to undrained conditions, especially at the slope base where compression is significant. Critical water pressures may arise even during non-exceptional precipitation events, leading to a toe breakout. Future studies on the afore-mentioned topics are therefore suggested to verify these assumptions. The findings of such studies may have useful implications for managing hazards to infrastructure and avoiding casualties related to the complex behaviour of deep-seated landslides.

Acknowledgements The author wishes to thank cantonal geologist C. Dénervaud for his collaboration and valuable discussion during the realization of this study; P. Perrochet for his useful comments; and R. Costa, M. De Boni, N. Siegenthaler and C. Zuffetti for their help in the field. Suggestions and comments from the reviewers were also particularly appreciated and helped to improve the paper.

Funding This research received no specific grant from any funding agency in the public, commercial or not-for-profit sectors.

Scientific editing by Cherith Moses; James Griffiths

References

Agliardi, F., Crosta, G.B. & Frattini, P. 2012. Slow rock-slope deformation. *In*: Clague, J.J. & Stead, D. (eds) *Landslide Types, Mechanisms and Modeling*. Cambridge University Press, Cambridge, 207–221.

Barton, N., Bandis, S. & Bakhtar, K. 1985. Strength, deformation and conductivity coupling of rock joints. *International Journal of Rock Mechanics and Mining Sciences & Geomechanics Abstracts*, **22**, 121–140.

Bonzanigo, L., Eberhardt, E. & Loew, S. 2007. Long-term investigation of a deep-seated creeping landslide in crystalline rock. Part I: Geological and hydromechanical factors controlling the Campo Vallemaggia landslide. *Canadian Geotechnical Journal*, **44**, 1157–1180.

Canton Grisons 2015. *Wald und Naturgefahren – Bericht 2015*. Annual report. Amt für Wald und Naturgefahren, Canton Grisons, Chur.

CSD Ingénieurs 2016. *Glissement rocheux des Buges à Boudry. Etude géologique générale et analyse du phénomène*. Technical report. CSD Ingénieurs, Yverdon-les-Bains.

Eberhardt, E., Bonzanigo, L. & Loew, S. 2007. Long-term investigation of a deep-seated creeping landslide in crystalline rock. Part II. Mitigation measures and numerical modelling of a deep drainage at Campo Vallemaggia. *Canadian Geotechnical Journal*, **44**, 1181–1199.

Eberhardt, E., Preisig, G. & Gischig, V. 2016. Progressive failure in deep-seated rockslides due to seasonal fluctuations in pore pressures and rock mass fatigue. *In*: Aversa, S., Cascini, L., Picarelli, L. & Scavia, C. (eds) *Landslides and Engineered Slopes. Experience, Theory and Practice: Proceedings of the 12th International Symposium on Landslides (Napoli, Italy, 12–19 June 2016)*. CRC Press, Boca Raton, FL, 121–136.

Elia, G., Cotecchia, F. *et al.* 2017. Numerical modelling of slope–vegetation–atmosphere interaction: an overview. *Quarterly Journal of Engineering Geology and Hydrogeology*, **50**, 249–270, https://doi.org/10.1144/qjegh2016-083

Frank, S. & Zimmermann, M. 2000. Rutschung 'Bätschen', Murgänge in der Wüechtenrus (Braunwald und Rüti, GL): eine Grossrutschung und ihre Folgeprozesse. *Bulletin für Angewandte Geologie*, **5**, 131–138.

Geoconsult 1985. *Les Buges: Etude géophysique du glissement 1984–1985*. Technical report. Centre de documentation du service des ponts et chaussées, Neuchâtel.

Geoconsult 1994. *Les Buges: Etude d'un glissement par inclinomètrie 1985–1993*. Technical report. Centre de documentation du service des ponts et chaussées, Neuchâtel.

Gischig, V. 2011. *Kinematics and failure mechanisms of the Randa rock slope instability (Switzerland)*. PhD thesis, ETH Zurich.

Gischig, V., Preisig, G. & Eberhardt, E. 2016. Numerical investigation of seismically induced rock mass fatigue as a mechanism contributing to the progressive failure of deep-seated landslides. *Rock Mechanics and Rock Engineering*, **49**, 2457–2478.

Grämiger, L.M., Moore, J.R., Gischig, V.S., Ivy-Ochs, S. & Loew, S. 2017. Beyond debuttressing: Mechanics of paraglacial rock slope damage during repeat glacial cycles. *Journal of Geophysical Research: Earth Surface*, **122**, 1004–1036.

Hungr, O., Leroueil, S. & Picarelli, L. 2014. The Varnes classification of landslide types, an update. *Landslides*, **11**, 167–194.

Király, L. 1969. Anisotropy and heterogeneity within jointed limestone. *Eclogae Geologicae Helvetiae*, **62**, 613–619.

Leroueil, S., Locat, J., Vaunat, J., Picarelli, L., Lee, H. & Faure, R. 1996. Geotechnical characterization of slope movements. *In*: Senneset, K. (ed.) *Landslides*. Balkema, Rotterdam, 53–74.

Loew, S., Gschwind, S., Gischig, V., Keller-Signer, A. & Valenti, G. 2017. Monitoring and early warning of the 2012 Preonzo catastrophic rockslope failure. *Landslides*, **14**, 141–154.

Meia, J. 1996. *Gorges de l'Areuse. Glissement des Buges. Géologie. Rapport de synthèse sur l'étude 1977–1996*. Technical report. Centre de documentation du service des ponts et chaussées, Neuchâtel.

Meia, J. & Becker, F. 1976. *Atlas géologique de la Suisse, feuille 1164 Neuchâtel*. Swiss Geological Survey. Federal Office of Topography swisstopo, Wabern bei Bern.

Menzel, L., Herbert, L. & Rohmann, M. 1999. *Mean annual actual evaporation 1973–1992. Hydrological Atlas of Switzerland*. Federal Office of Topography swisstopo, Wabern bei Bern.

Meteoswiss 2017. *CLIMAP-net: portail de données météorologiques*. Federal Office of Meteorology and Climatology Meteoswiss, Geneva.

Pánek, T. & Klimeš, J. 2016. Temporal behavior of deep-seated gravitational slope deformations: A review. *Earth-Science Reviews*, **156**, 14–38.

Parriaux, A., Bonnard, C. & Tacher, L. 2010. *Glissements de terrain: hydrogéologie et techniques d'assainissement par drainage. Guide Pratique*. Federal Office for the Environment (FOEN), Bern.

Pasquier, F., Burkhard, M., Mojon, P.-O. & Gogniat, S. 2013. *Geological Atlas of Switzerland: 1163 Travers*. Swiss Geological Survey. Federal Office of Topography swisstopo, Wabern bei Bern.

Preisig, G., Eberhardt, E. *et al.* 2014. Development of connected rock mass permeability through hydraulic fracture propagation and shearing accompanying fluid injection. *Geofluids*, **15**, 321–337.

Preisig, G., Gischig, V., Eberhardt, E. & Hungr, O. 2015. Hydromechanical versus seismic fatigue in progressive failure of deep-seated landslides. *In*: *13th ISRM International Congress of Rock Mechanics (Montréal, Canada, 10–13 May 2015)*. International Society for Rock Mechanics.

Preisig, G., Eberhardt, E., Smithyman, M., Preh, A. & Bonzanigo, L. 2016. Hydromechanical rock mass fatigue in deep-seated landslides accompanying seasonal variations in pore pressures. *Rock Mechanics and Rock Engineering*, **49**, 2333–2351.

Rey, T. 2015. *Etude structurale du Jura Neuchâtelois (Suisse)*. MSc thesis, Université de Fribourg.

Sartori, M., Baillifard, F., Jaboyedoff, M. & Rouiller, J.D. 2003. Kinematics of the 1991 Randa rockslides (Valais, Switzerland). *Natural Hazards and Earth System Sciences*, **3**, 423–433.

Schardt, H. & Dubois, A. 1902. *Description géologique de la région des Gorges de l'Areuse (Jura neuchâtelois)*. Bulletin de la Société Neuchâteloise des Sciences Naturelles, **XXX**.

SIA VSS 2011. *SN 670 010: Reconnaissance et essais géotechniques, Paramètres géotechniques*. Swiss Association of Road and Transportation Experts, Zurich.

Smethurst, J.A., Clarke, D. & Powrie, W. 2012. Factors controlling the seasonal variation in soil water content and pore water pressures within a lightly vegetated clay slope. *Géotechnique*, **62**, 429–446.

Smethurst, J.A., Smith, A. *et al.* 2017. Current and future role of instrumentation and monitoring in the performance of transport infrastructure slopes. *Quarterly Journal of Engineering Geology and Hydrogeology*, **50**, 271–286, https://doi.org/10.1144/qjegh2016-080

Strozzi, T., Delaloye, R., Kääb, A., Ambrosi, C., Perruchoud, E. & Wegmüller, U. 2010. Combined observations of rock mass movements using satellite SAR interferometry, differential GPS, airborne digital photogrammetry, and airborne photography interpretation. *Journal of Geophysical Research*, **115**, 11.

swisstopo 2017. *swissALTI3D: le modèle de terrain à haute résolution de la Suisse*. Federal Office of Topography, Wabern bei Bern, https://shop.swisstopo.admin.ch/fr/products/height_models/alti3D

Tacher, L., Bonnard, C., Laloui, L. & Parriaux, A. 2005. Modelling the behaviour of a large landslide with respect to hydrogeological and geomechanical parameter heterogeneity. *Landslides*, **2**, 3–14.

Wolter, A., Gischig, V., Stead, D. & Clague, J.J. 2016. Investigation of geomorphic and seismic effects on the 1959 Madison Canyon, Montana, Landslide using an integrated field, engineering geomorphology mapping, and numerical modelling approach. *Rock Mechanics and Rock Engineering*, **49**, 2479–2501.